THE JOURNAL OF PHYSICAL CHEMISTRY C
A JOURNAL OF THE AMERICAN CHEMICAL SOCIETY

pubs.acs.org/JPCC

Article

Influence of CO_2 on Nanoconfined Water in a Clay Mineral

Kristoffer W. Bø Hunvik,* Rodrigo José da Silva Lima, Alexsandro Kirch, Patrick Loch, Paul Monceyron Røren, Martin Hoffmann Petersen, Svemir Rudić, Victoria García Sakai, Kenneth Dahl Knudsen, Caetano Rodrigues Miranda, Josef Breu, Jon Otto Fossum,* and Heloisa N. Bordallo*

Cite This: *J. Phys. Chem. C* 2022, 126, 17243−17254

Read Online

ACCESS | Metrics & More | Article Recommendations | Supporting Information

ABSTRACT: Developing new technologies for carbon sequestration and long-term carbon storage is important. Clay minerals are interesting in this context as they are low-cost, naturally abundant, can adsorb considerable amounts of CO_2, and are present in storage sites for anthropogenic carbon. Here, to better understand the intercalation mechanisms of CO_2 in dehydrated and hydrated synthetic Na-fluorohectorite clay, we have combined powder X-ray diffraction, inelastic and quasi-elastic neutron scattering, and density functional theory calculations. For dehydrated Na-fluorohectorite, we observe no crystalline swelling or spectroscopic changes in response to CO_2, whereas for the hydrated case, damping of the librational modes related to the intercalated water was clearly observed. These findings suggest the formation of a more disordered water coordination in the interlayer associated with highly confined water molecules. From the simulations, we conclude that intercalated water molecules decrease the layer−layer cohesion energy and create physical space for CO_2 intercalation. Furthermore, we confirm that interlayer confinement reduces the Na^+ hydration number when compared to that in bulk aqueous water, which may allow for proton transfer and hydroxide formation followed by CO_2 adsorption in the form of carbonates. The experimental results are discussed in the context of previous and present observations on, a similar smectite, Ni-fluorohectorite, for which it is established that CO_2 attaches to the edge of nickel hydroxide islands present in the interlayer.

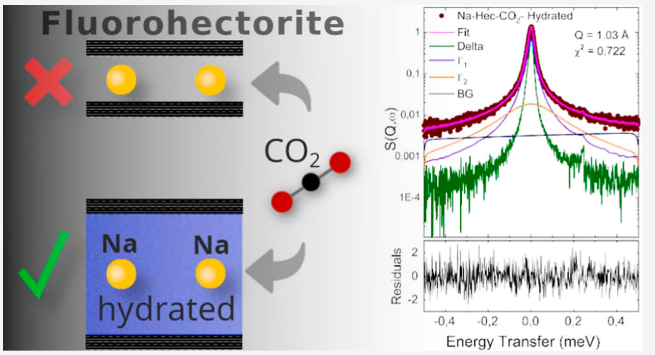

INTRODUCTION

Investigating the dynamics of molecules in nanoconfined media is essential to understand transport properties in 2D nanomaterials. The role of water is especially important for clay minerals because of their significance in soils[1,2] and their use in many different applications, such as construction materials,[3] dye remediation,[4] drug delivery,[5−8] or as engineered barriers in radioactive waste management.[9,10] For these applications, it is important to control and monitor their swelling behavior and, hence, have an understanding of these materials at a molecular level.

Clay minerals (especially expandable clays such as smectites or pillared clays) can be a more sustainable alternative to aqueous amine solutions, synthetic solid sorbents such as activated carbon, zeolites, and metal−organic frameworks for carbon capture and storage. This is due to their low cost, natural abundance, and ability to sorb CO_2. Indeed, clay minerals have been proposed as being useful in cyclic gas separation processes since the regeneration from their weaker adsorption sites requires less energy input than that from stronger adsorption sites in materials such as the benchmark material zeolite 13X.[11] As large quantities of clay minerals are present in the caprock formation of reservoirs intended for anthropogenic CO_2 capture,[12] understanding molecular interactions between water and CO_2 at clay mineral interfaces is paramount to ensure the long-term stability of such reservoirs.

Smectites are 2:1 layered clay minerals with layers consisting of an octahedral sheet sandwiched between two tetrahedral sheets, where isomorphic substitutions of metal cations in either the octahedral or tetrahedral sheets produce a net negative charge in the clay layer which is balanced by interlayer cations. Smectites are known to swell in response to, and adsorb, both water[13−15] and CO_2.[11,16−21,21−25] As a result of its natural abundance and also the possibility of melt-synthesizing high-purity samples,[26] Na^+-intercalated smectites have been by far the most studied.[26−30] For an expandable clay mineral such

Received: May 12, 2022
Revised: September 15, 2022
Published: October 3, 2022

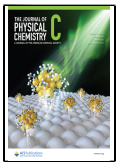

as smectite, water enters the 2D nanoporous interlayer and expands the clay in discrete steps. It is now widely accepted that for the case of one water layer (1 WL), the interlayer cation resides close to the tetrahedral sheet, with a ninefold coordination with six basal oxygens and three water molecules, while in the two-water layer (2WL) state, the cation resides at the center of the interlayer coordinating with six water molecules.[27] For hectorite (Hec) with either/or OH^- and F^- anionic substitutions, it has been found that the hydrophobicity increases with fluorination, resulting in a reduced water uptake.[14] For CO_2 adsorption in Na^+-intercalated smectites, the results in the literature are "scattered". Dried fluorinated Na-Hec readily swells in response to CO_2[16,17] and adsorbs a considerable amount,[31] whereas for natural dehydrated Na-smectites, no swelling has been detected in response to CO_2.[11,23,24,32,33] Under such conditions, only a limited amount of CO_2 adsorption occurs on the external surfaces. From experimental[11,19,20,22−24,34] and molecular simulation[24,32−36] studies, it is now assumed that smaller cations (such as Na^+) require a sub-monolayer of water to "prop open" the interlayer before CO_2 adsorption occurs, while for larger cations (such as Cs^+ and NH_4^+), CO_2 is readily adsorbed even in the absence of water. Similar observations have been made for Ni-Hec, which has a corrensite structure, where under anhydrous conditions, the more open chlorite-like layers adsorb CO_2, and the more closed smectite layers do not.[18,37] Thus, we can argue that adsorption of CO_2 in the interlayer of smectites is not only governed by the cationic species within but also the clay sheets. By tuning the OH^- and F^- anionic substitutions, simulations have shown that the total intercalation of CO_2 and H_2O decreases with fluorination, whereas the mole fraction $CO_2/(H_2O + CO_2)$ increases, and the maximum uptake is observed at 1 WL.[32] By lowering the surface charge of the clay sheets, increased adsorption and a lower pressure threshold for adsorption were observed for Ni-Hec.[37] This is a result of the weaker electrostatic forces acting between the layers and the lower density of interlayer species allowing for more CO_2 within the interlayer. As for the organization of CO_2 within the interlayer, in the 1 WL state, nuclear magnetic resonance[20] and simulations[32,38,39] have demonstrated that CO_2 orients itself parallel to the clay surface in the midplane of the interlayer.

In this work, we carried out inelastic and quasi-elastic neutron scattering experiments (INS and QENS) and powder X-ray diffraction (PXRD), to study the influence of water (swelling) and CO_2 (adsorption) on the synthetic smectites Na- and Ni-fluorohectorite (Hec). Combining structural and spectroscopic data gives a more complete chemical analysis of these systems. The unique sensitivity of neutron spectroscopy to hydrogen,[40] lack of selection rules, and high neutron penetrability through the sample environment[41] allow a better understanding of how the layer charge, interlayer cations, and geometrical confinement affect the conformation of the water molecules.[42,43] In addition, QENS provides insights into the self-diffusion processes of the hydrogenous species on the ps to ns timescale.[44] The experimental results are complemented by density functional theory (DFT) calculations to evaluate the electrostatic environment involved in the adsorption of CO_2 in the interlayer region. In the present work, we use a similar approach to investigate Na-Hec as that previously carried out for Ni-Hec,[18] where the sample is prepared in the dried (at 150 °C under dynamic vacuum) and hydrated [equilibrated 43% relative humidity (r.h.)] states.

EXPERIMENTAL SECTION

Materials. Na-Hec with the stoichiometric composition of $Na(Mg_5Li)Si_8O_{20}F_4$ was prepared via melt synthesis,[45] followed by annealing (6 weeks, 1045 °C) to improve charge homogeneity and phase purity.[26] Ni-Hec was prepared by cation exchange of Na-Hec with 0.2 M nickel-acetate solution (>10-fold excess of the cation exchange capacity, 5 times).[46] The exchanged Ni-Hec was washed five times with Millipore water. All the samples in this work had a nominal charge of 0.5 e^- per formula unit (pfu).

For the reported experiments, dried Na-Hec used for PXRD was prepared under vacuum (10^{-2} mbar) at 150 °C for 2 h, while due to the larger mass required for the INS and QENS experiments, Na and Ni-Hec samples were placed under high vacuum (10^{-6} mbar) at 145 ± 15 °C for 7 h (INS, Na-Hec sample) or at 145 ± 15 °C for 13 h (QENS, Ni-Hec) or 17 h (QENS, Na-Hec). Hydrated Ni-Hec and Na-Hec were obtained by placing samples for 5 weeks at 43% r.h. in a desiccator with saturated K_2CO_3 solution.

In situ Powder X-ray Diffraction. PXRD measurements were carried out at NTNU (Trondheim, Norway) using an in-house X-ray scattering instrument, attached to a Xenocs stationary electron impact source with a copper anode, producing $K\alpha$ radiation (1.5406 Å). The scattered intensity was recorded using a two-dimensional Dectris Pilatus3 R 200 K detector. The samples were mounted in a high-pressure sample cell based on a designed thin-walled glass capillary-based cell.[47] Temperature control was provided by contact of the capillary with a temperature-regulated copper plate where cartridge heaters, Peltier elements, and a circulation bath controlled the temperature. The sample cell was connected to a gas handling system providing vacuum from a rotary vane pump (10^{-2} mbar) or pressurized CO_2 with 99.9992% purity.

Inelastic Neutron Scattering (INS) and Quasi-Elastic Neutron Scattering (QENS). INS spectra were recorded on the TOSCA spectrometer[48−50] at the ISIS facility, Rutherford Appleton Laboratory, UK. TOSCA is an indirect geometry time-of-flight spectrometer spanning an energy-transfer range of up to 4000 cm^{-1} in neutron energy loss (E_T) with a spectral resolution of 1.25% E_T.[48] Dried and hydrated Na-Hec samples were placed in an aluminum foil sachet and mounted in stainless steel cylinders. The sample holder was then mounted on a centerstick connected to a gas handling system. Prior to measurements, the cell was leak-tested to 50 bar helium that was pumped away in the case of the dried samples and leaked slowly down to atmospheric pressure in the case of the hydrated samples (to preserve the initial humidity). Both samples were measured as is and at 44 bar of CO_2 exposure. Each exposure was achieved by first heating up the sample to room temperature and exposing the sample to CO_2 grade 99.9995% for 20 min. At this point, the sample cell was closed and sealed off from external CO_2 gas pressure. Subsequently, in order to minimize thermal effects, the sample was cooled down, and the measurements were recorded at $T < 20$ K. Each INS measurement lasted around 6−8 h, that is, until a good signal to noise ratio was obtained. The data were reduced using the software package Mantid.[51] After subtracting the signal from the empty cell, the spectra were scaled by the sample mass. After exposure to CO_2, the signal was normalized to have the same area under the curve as in the initial spectrum.

QENS experiments were conducted on the indirect-geometry time-of-flight spectrometer IRIS[52] also at the ISIS

https://doi.org/10.1021/acs.jpcc.2c03310
J. Phys. Chem. C 2022, 126, 17243−17254

facility. The instrument was operated in the offset mode using the (002) Bragg reflection of pyrolytic graphite analyzers. In this configuration, the elastic energy resolution of the instrument was 17.5 μeV achieved by neutrons scattered with λ = 6.66 Å. This resolution is constant over the entire Q-range of 0.4−1.96 Å^{-1} (angular scattering range of 25° ≤ 2Θ ≤ 160°). Between 0.67 and 1.22 g of each sample was loaded into annular cylindrical aluminum sample holders with inner diameter 21 mm, wall thickness 1.6 mm, and sample space thickness 0.5 mm. The temperature of the samples was maintained at 300.0 ± 0.1 K using a closed-cycle refrigerator. During CO_2 exposure, the samples were held at 40−43 bar of CO_2 pressure (grade 99.9995%). Typical counting times were ∼5−15 h for each state depending on the hydrogen content in the sample. In addition to the samples themselves, spectra of the empty cell and a vanadium standard were collected in order to determine the instrument background and instrumental resolution, respectively. The data were reduced using the software package Mantid[51] and analyzed using either Dave software[53] or the newly developed minimal model approach.[54] By using Dave, prior information of the system is essential to determine the specific number of Lorentzian needed to analytically describe the system dynamics, which can be obtained from different experimental techniques,[55] while in the minimal model, the multiscale relaxation measured by QENS is analyzed using a purely mathematical approach. Bragg reflections, Figure S1, were eliminated from the data prior to the analysis.

Density Functional Theory (DFT). DFT calculations were performed with the Siesta package[56] to investigate molecular conformations and adsorption energies in the Hec interlayer region. State-of-the-art DFT developed by Berland and Hyldgaard[57] was employed to take into account van der Waals interactions. A double-zeta polarized basis and converged 400 Ry mesh cutoff were used. We considered the crystallographic structure used in our previous study[18] with unit cell dimensions 9.2 × 10.7 × 12.0 Å and 78 atoms, under fully periodic boundary conditions. The positions of ions and molecules in the interlayer space were optimized with the conjugated gradient method until the forces were less than 0.01 eV/Å. During this process, the atoms of the layered structure were kept fixed. Molecular conformations were obtained through ab initio molecular dynamics considering a 10 ps simulation, 1 fs time step, and 300 K temperature controlled with the Nosé−Hoover thermostat.

To evaluate charge rearrangements in the system, we determined the charge difference as given by

$$\rho_{diff} = \rho_{doped} - \rho_{bulk} \quad (1)$$

where ρ_{doped} and ρ_{bulk} are the electronic charges for the phyllosilicate with and without the Li substitutional atom in the octahedral sheet, respectively.

The molecular adsorption on the Na atom in the confined space was evaluated by determining the adsorption energy given using the following equation

$$E_{ads} = E_{total} - E_1 - E_{mol} \quad (2)$$

where E_{total} is the total energy of the system containing all the molecules, E_1 considers the system with one molecule missing, and E_{mol} is the energy of that isolated molecule.

RESULTS AND DISCUSSION

In Situ Powder X-ray Diffraction. Figure 1 shows the evolution of the (001) Bragg reflection for the dried and hydrated Na-Hec at 43% r.h. upon CO_2 exposure. Initially, this reflection for the dried Na-Hec is found at q = 0.65 Å^{-1}, corresponding to a basal spacing of 9.6 Å, which indicates complete collapse to 0 WL.[26,27] When exposed to CO_2, there is no appreciable change in the pattern, even after 13 days of continuous exposure. Absence of swelling for a dehydrated Na-smectite is in line with other previous observations and simulations on montmorillonite and Hec.[24,32] For Na-Hec equilibrated at 43% r.h., the (001) Bragg reflection is initially found at 0.515 Å^{-1}, giving a basal spacing of 12.2 Å, corresponding to the 1 WL state.[26,27] After exposing the sample to CO_2, only a very small and insignificant change in Bragg spacing swelling of 0.06 Å is observed, which is the detection limit of the instrument. These results suggest that 0 WL and 1 WL states are stable energy minimas, and CO_2 does not cause further swelling of Na-Hec.

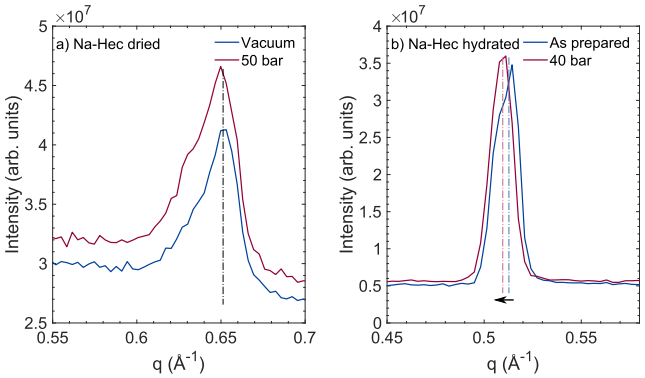

Figure 1. X-ray diffraction pattern of the (001) Bragg reflection for (a) dried and (b) hydrated Na-Hec at 300 K for the initial and CO_2-exposed states. The horizontal lines indicate the center of the reflection. Figure (a) has been reprinted with permission from ref 18. Copyright 2020 American Chemical Society.

It is interesting to note the striking difference in behavior after CO_2 exposure when comparing the Na-Hec samples to previously published data on similar Ni-Hec samples; swelling was clearly observed in the latter, with an increase in d-spacing from 22.8 to 24.6 Å in the dried case and 29.6−30.1 Å in the hydrated case.[18] This effect was related to the existence of ordered interstratification of strictly alternating chlorite-like and smectite-like layers[46] in Ni-Hec resulting in inclusion of CO_2 within the chlorite-like layers.[18] Furthermore, we also note that different from the present work, a crystalline swelling of about 30% in relation to the dried state has been previously reported in Na-Hec samples of commercial origin.[16,17] The samples synthesized at the University of Bayreuth studied in the present work have been proven to be of superior quality compared to other clays.[26] We can only speculate how the difference between the present work and refs 16 and 17 can be attributed to sample origin, charge, phase purity, and preparation methods including cation exchange (Li^+ to Na^+ for the commercial samples), drying procedures, and sample cells.

Inelastic Neutron Scattering. INS spectra of pristine Na-Hec both in the dried and equilibrated at 43% r.h. states are presented in Figure 2. The difference spectrum, obtained by

https://doi.org/10.1021/acs.jpcc.2c03310
J. Phys. Chem. C 2022, 126, 17243−17254

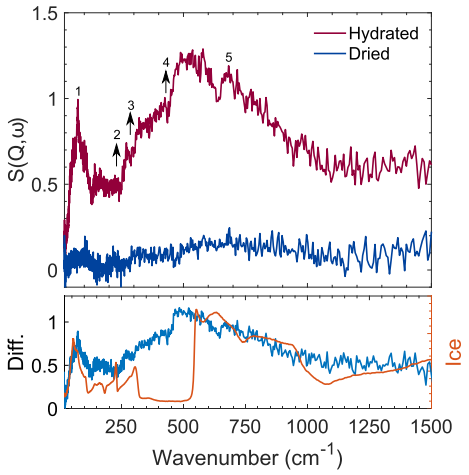

Figure 2. INS experimental spectra of the Na-Hec in the dried (145 °C under dynamic vacuum for 7 h) and hydrated state (equilibrated at 43% r.h.) with the corresponding difference spectrum compared with the INS spectrum of ice Ih as a standard reference (in orange and scaled by the right axis). Numbers and arrows are used to highlight the modes summarized in Table 1. The onset of the librational features, commonly referred to as the librational edge, was used to characterize the interlayer cation.[43,58,59] The spectra were recorded at $T < 20$ K.

subtracting the minimal contribution of the clay lattice (dried sample) from that of the 1 WL hydrated clay, shows only the contribution from confined interlayer water. A tentative assignment of the observed modes is given in Table 1. For

Table 1. Proposed Assignment of the Vibrational Modes Observed Using Inelastic Neutron Scattering (INS) for Hydrated Na-Hec with Numbering Given in Figure 2

feature number	position (cm^{-1})	suggested assignment
1	73 (broad)	H_2O; acoustic
2	250 (rise)	H_2O; librational edge
3	300 (rise)	H_2O; librational edge
4	446 (rise)	H_2O; librational edge
5	680 (broad)	H_2O

the dried sample (heated at 145 °C under dynamic vacuum), only a very low intensity is observed, where the tiny structures around 80 cm^{-1} and between 500 and 1000 cm^{-1} can be attributed to a minor amount of residual water left in the sample. Of more interest is the comparison between the spectrum of interlayer water in 1 WL Na-Hec and the one previously reported for 2 WL Ni-Hec,[18] where the former appears to have a less well-defined librational edge. The difference arises not only because the two samples are in different hydration states but also because the cations have different hydration enthalpies, leading to a different interaction with the water molecules.[30] For instance, and in full agreement with previous observations by QENS for Hec intercalated with Na^+ and Ni^{2+}, the lower Na-Hec librational edge indicates that water experiences a less constrained environment in this sample.[30,60] Similar observations have been found for montmorillonite and beidellite,[43] where the type of cation significantly affects the position of the librational modes leading to a more constrained water environment for divalent high-hydration enthalpy Mg^{2+}, as opposed to Na^+. Furthermore, the less-developed low-energy edge reported for Na^+ was attributed to either different distributions of librational motions or a modified disordered state with multiple environments for the interlayer water.[43] Since melt-synthesized Na-Hec is known to form a well-defined 1 WL state,[27] the lower edge observed here can be attributed to the presence of two water populations in the sample, that is, water directly coordinated with the cation and free interlayer water. From thermal gravimetric analysis[46] and gravimetric adsorption of water[61] in Na-Hec, it is known that there are approximately 4.2 water molecules per cation present at 1 WL. Moreover, in the 1 WL state, an inner-sphere complex is observed, with Na^+ being in direct contact with basal oxygen atoms on one side, due to Coulomb attraction, and coordinated by three water molecules on the other side.[27] This suggests that at least 1.2 water molecules per cation are non-coordinated. This is further discussed in the next section in conjunction with the QENS data analysis.

Figure 3 displays the INS spectra of the samples after exposure to 44 bar of CO_2 pressure at room temperature and being subsequently cooled down to $T < 20$ K. For dried Na-

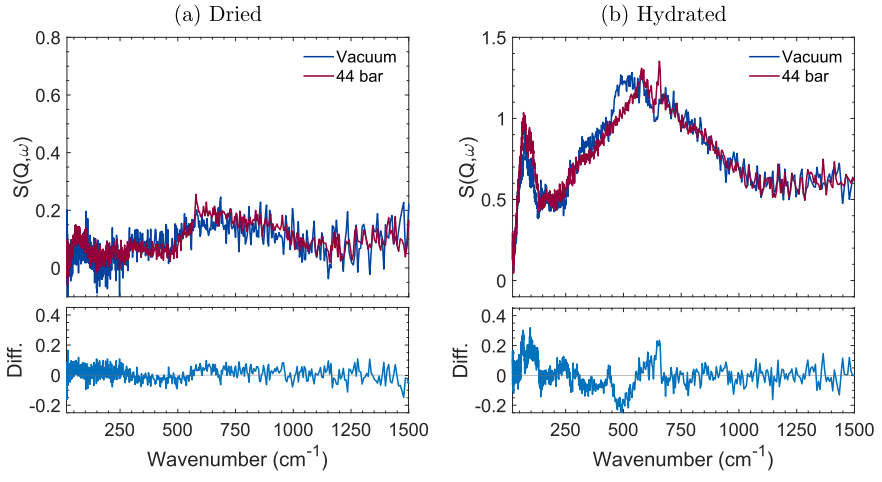

Figure 3. INS experimental spectra of (a) dried and (b) hydrated Na-Hec in the initial state and after exposure to 44 bar of CO_2 with the corresponding difference spectra given below. Loading of CO_2 was performed at room temperature, and the spectra were recorded at $T < 20$ K. Figure (a) has been reprinted with permission from ref 18. Copyright 2020 American Chemical Society.

https://doi.org/10.1021/acs.jpcc.2c03310
J. Phys. Chem. C 2022, 126, 17243−17254

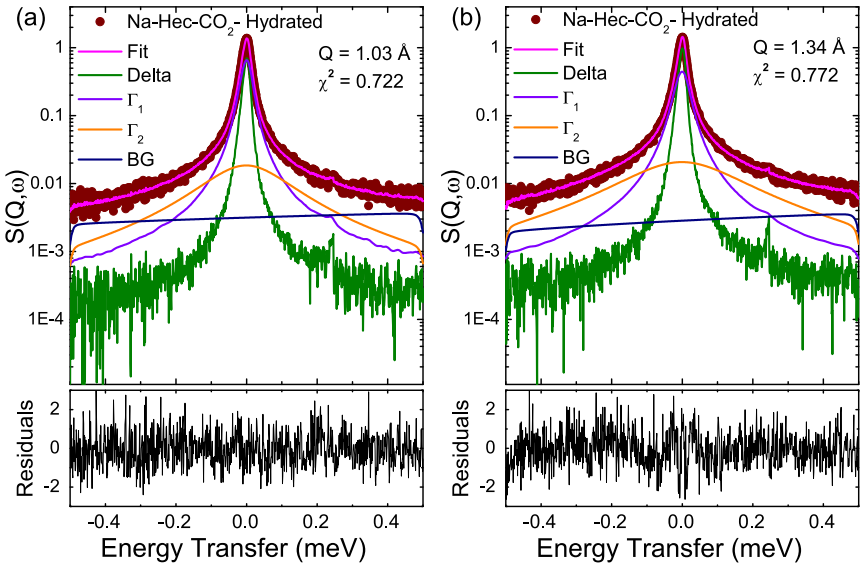

Figure 4. QENS spectra collected at 300 K for hydrated Na-Hec after CO_2 exposure (40 bar). (a) Q = 1.03 and (b) Q = 1.34 Å^{-1}, including the best fits, its QE components (Γ_1 describing the more confined cationic water and Γ_2 describing the faster interlayer water), and background. The vanadium data shown (delta) was used in the fitting and provides an experimental measure of the IRIS instrument energy resolution.

Hec, 44 bar CO_2 exposure (Figure 3a) induces minor changes to the spectrum. This is in full agreement with the diffraction data (Figures 1 and S1), further confirming that under these experimental conditions, CO_2 does not intercalate in dried Na-Hec. However, for hydrated Na-Hec (Figure 3b), changes are more evident and better emphasized in the difference spectrum. An excess of energy is observed at 64 cm^{-1} and at 95 cm^{-1}, with a broad shoulder centered at 117 cm^{-1}, and additional intensity losses at 141 and 297 cm^{-1} and 355 and 490 cm^{-1}. Furthermore, a sharp peak appears at 655 cm^{-1}. These changes suggest a disruption of the modes of either both or one of the two water populations, possibly owing to a more disordered coordination of the interlayer water with the Na^+ cation. This is in line with observations for montmorillonite and Hec at 1 WL, where it has been suggested that CO_2 can intercalate and disrupt the cation and the H_2O dynamics through direct Na−CO_2 association.[20,38,39] On the other hand, since no significant swelling is observed, CO_2 would have to replace H_2O in the hydration sphere. This is, however, not energetically favorable. Thus, we can argue that the interaction may be with the free interlayer water, that is, the water that is not coordinated with cations. Additionally, the observed change in the librational edge for hydrated Na-Hec is more dramatic than that for hydrated Ni-Hec.[18] In fact, in the latter, no change was observed for hydrated Ni-Hec after CO_2 exposure (Figure 7 in ref 18), suggesting that the water present in the hydrated smectite layers in Ni-Hec is less disturbed. This is possibly due to the higher hydration enthalpy of the Ni^{2+} cation creating a more stable environment for the interlayer water. Still, the Ni-Hec from the previous study was in the 2 WL state and showed the presence of other hydrogenous species in the interlayer, so a direct comparison of the spectra is not straightforward.

With regard to the mode assignments, the vibrations observed between 60 and 120 cm^{-1} and at 655 cm^{-1} were also observed for both dried and hydrated Ni-Hec exposed to CO_2 (Figures 6 and 7 ref 18). In that study, it was suggested that these modes may come either from bicarbonate formation or by the formation of a new ordered water population in the clay. As bicarbonates are not commonly observed for clay minerals exposed to CO_2 under similar experimental conditions,[62] it is more likely that this is due to a new confined water population in the clay. Indeed, similar observation of water confinement in UO_2F_2 with a peak at 778 cm^{-1} was attributed to a librational phonon mode originated from confined water within the van der Waals gap.[63] In the present case and as suggested by simulations,[39] it is possible that CO_2 clustering in the interlayer space induces a different entrapment of the water molecules.

Quasi-Elastic Neutron Scattering: Differences in the Water Diffusion. QENS was used to probe how the mobility of the confined water molecules is disturbed by the adsorbed CO_2 in both dried and hydrated Na- and Ni-Hec. We conclude that the slight decrease in the elastic signal followed by a minimal increase in the quasi-elastic broadening after CO_2 exposure supports the idea that a new highly confined water population develops in dried Ni-Hec after CO_2 exposure, Figure S3. On the other hand, no variation in the elastic signal or quasi-elastic broadening was detected for dried Na-Hec, Figure S2. Regarding the hydrated samples, a different picture emerges; the spectra for Ni-Hec before and after exposure are seemingly unchanged, Figure S4, whereas a small variation in the quasi-elastic spectra at the lowest Q-value can be observed for Na-Hec, Figure S5. This can be understood as follows: the negligible crystalline swelling for hydrated Na-Hec suggests that the 1 WL state is an energy minimum and that the interaction with CO_2 is not able to change it. Moreover, based on the observation from INS and QENS, it is safe to say that the 1 WL state still provides a large enough space to accommodate the dynamic size of the CO_2 molecule, explaining the changes in the INS data and the QENS data at 0.69 Å^{-1}. The presence of CO_2 in the collapsed 0 WL Na-Hec is not permitted because the swelling must accommodate the real size of the CO_2 molecule (3.3 Å).[64] Thus, for the dried Na-Hec, the absence of swelling due to CO_2 exposure demonstrates that the interaction with the clay surface or Na cation alone is not sufficient for crystalline swelling in response

https://doi.org/10.1021/acs.jpcc.2c03310
J. Phys. Chem. C 2022, 126, 17243−17254

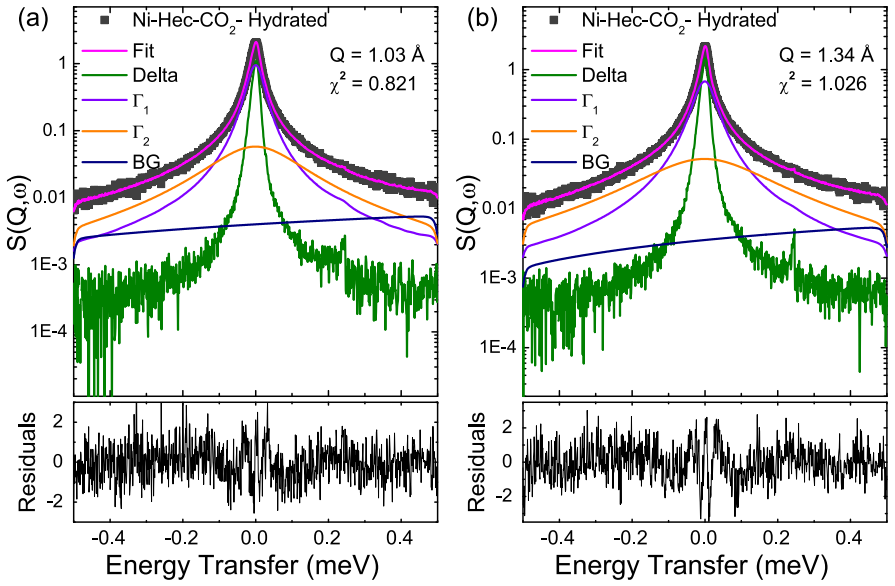

Figure 5. QENS spectra collected at 300 K for hydrated Ni-Hec after CO_2 exposure (43 bar). (a) Q = 1.03 and (b) Q = 1.34 $Å^{-1}$, including the best fits, its QE components (Γ_1 describing the more confined cationic water and Γ_2 describing the faster interlayer water), and background. The vanadium data shown (delta) was used in the fitting and provides an experimental measure of the IRIS instrument energy resolution.

to CO_2, and the presence of water is required, in line with previous observations.[24,32,33]

Now, we consider the QENS data collected for hydrated Ni- and Na-Hec at 300 K. Since individual trajectories of all relaxation processes cannot be distinguished, the systems were assumed to be dynamically heterogeneous, and the different types of hydrogen motions were superimposed independently. Thus, the scattering function, $S(Q, \omega)$, can be expressed as

$$S(Q, \omega) = \left[\mathrm{DWF}\left(A_0(Q)\delta(\omega) + (1 - A_0(Q))\sum_{i=1}^{n} L_i (\Gamma, \omega)\right) \otimes R(Q, \omega)\right] + B(Q) \quad (3)$$

where DWF is the Debye−Waller factor. $A_0(Q)$, defined as the averaged elastic incoherent structure factor (EISF), describes the probability that a particle is located in the same spatial volume after a time interval, t. The term $\sum_{i=1}{}^{n}L_i(\Gamma,\omega)$ is the sum of Lorentzians describing the broadened energy distribution, corresponding to distinct relaxation processes observed within the resolution of the instrument, $R(Q, \omega)$. The delta function, $\delta(\omega)$, describes those particles which are immobile within the timescale of the IRIS spectrometer. $B(Q)$ is a background function. Here, the data were fitted using two Lorentzian functions: a narrow one, defined as (Γ_1), describing the slower and more confined cationic water plus a broader Lorentzian function, named (Γ_2), describing the faster interlayer (free bulk-like) water. The initial value for (Γ_1) and (Γ_2) was taken from Larsen et al.[30] and Berg et al.[55] Representative results from this procedure are shown in Figures 4 and 5, including the best fits and QE components (Γ_1 and Γ_2) plus a linear background.

The self-diffusion coefficient, D_t, average residence time between jumps, τ_0, and the mean jump distance, L, defined as $D_t = \frac{L^2}{6\tau_0}$ were obtained from the analysis of the half width at half-maximum (Γ, HWHM) versus Q^2 using the expression for the random jump diffusion[65]

$$\Gamma(Q) = \frac{D_t Q^2}{1 + D_t Q^2 \tau_0} \quad (4)$$

The results are summarized in Table 2, and the fits are shown in Figures 6 and 7. The areas obtained from the fits describe amounts of each water population for the Na-Hec and Ni-Hec samples after CO_2 exposure.

Table 2. Parameters Obtained from Fitting the HWHMs Using Equation 3 Describing a Random Jump Diffusion for Na-Hec and Ni-Hec before and after Exposure to CO_2[a]

sample	D (10^{-9} m^2/s)	τ_0 (ps)	L (Å)
interlayer (bulk-like) water (fixed)	2.49 ± 0.07	1.57 ± 0.12	1.53
Na-Hec hydrated	0.21 ± 0.01	16 ± 2	1.42
Na-Hec hydrated CO_2	0.21 ± 0.01	16 ± 2	1.42
Ni-Hec hydrated	0.36 ± 0.02	11 ± 1	1.54
Ni-Hec hydrated CO_2	0.36 ± 0.02	11 ± 1	1.54

[a]Interlayer water is the water that is not directly coordinated with the cation.

Even if changes in the dynamics in the hydrated samples before and after exposure to CO_2 were not detected, a new and important insight was obtained.

(i) First, the smaller contribution from the residual water in Na-Hec compared to Ni-Hec indicates that the samples were not fully dried, explaining the observation of a tiny signal in the INS spectra of Na-Hec (Figure 3). This shows that these samples can easily retain surface water, which, due to the sensitivity of neutron scattering to the hydrogen atoms, can be readily observed. Surface water is the water found on the external surfaces or interparticle surfaces rather than in the interlayer space on the clay mineral.

(ii) Second, differences in the reduced diffusion coefficient and residence times observed between Na-Hec and Ni-

https://doi.org/10.1021/acs.jpcc.2c03310
J. Phys. Chem. C 2022, 126, 17243−17254

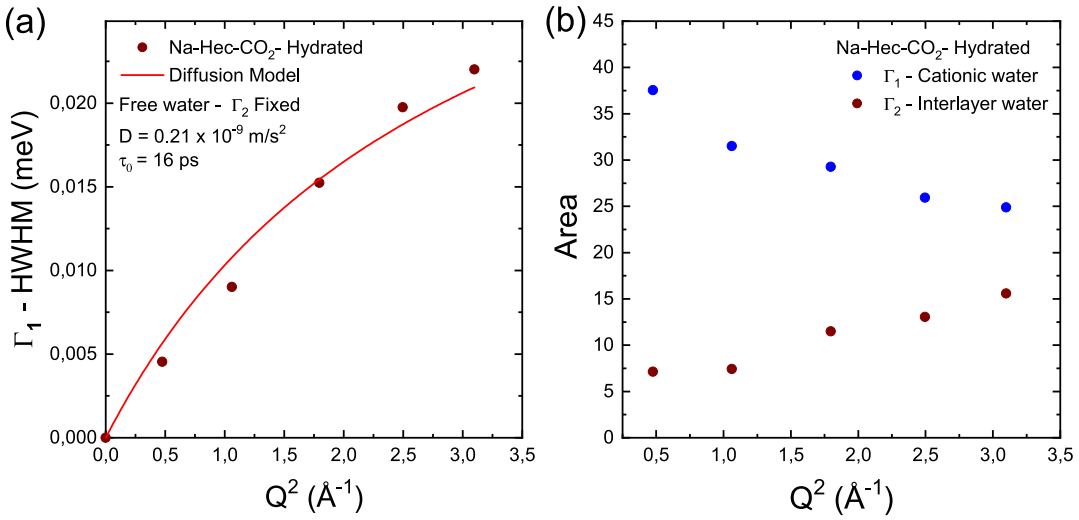

Figure 6. Evolution of the HWHM of the quasielastic broadening, Γ_1 confined cationic water, as a function of Q^2 obtained for the Na-Hec after CO_2 exposure (43 bar) and modeled using the theory developed to describe random jump diffusion.[65]

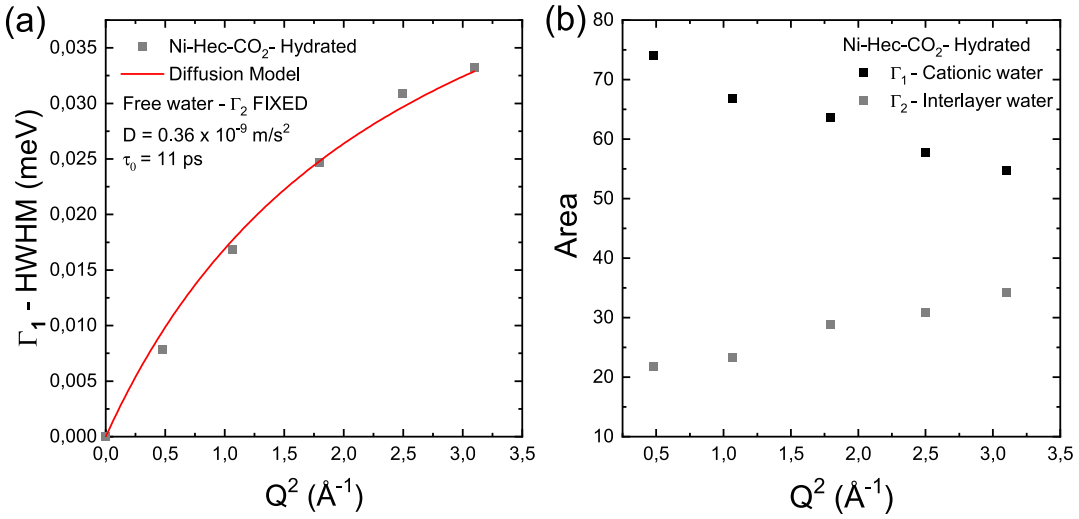

Figure 7. Evolution of HWHM of the quasielastic broadening, Γ_1 confined cationic water, as a function of Q^2 obtained for the Ni-Hec after CO_2 exposure (40 bar) and modeled using the theory developed to describe random jump diffusion.[65]

Hec, $0.21 \pm 0.01 \times 10^{-9}$ m^2/s versus $0.36 \pm 0.02 \times 10^{-9}$ m^2/s—Table 2, can be attributed not only to the water molecules attached to the interlayer cation but also to interstratified nickel hydroxide species.[18] Furthermore, the higher and similar diffusion coefficient reported for commercial Na- and Ni-Hec at 1WL, namely, $0.44 \pm 0.22 \times 10^{-9}$ m^2/s versus $0.47 \pm 0.03 \times 10^{-9}$ m^2/s in ref 30, can be explained by the resolution (≈100 μeV) of the time-of-flight spectrometer, which is unable to distinguish the contribution from the water molecules that interact directly with the interlayer cation from those coordinated with the interstratified nickel hydroxide species $[Ni(OH)_{0.83}(H_2O)_{1.17}]_{0.37}$. This is a well-known behavior as previously reported for natural smectite clay minerals.[66]

(iii) Third, by comparing the values of the jump distance L obtained for all samples with those of proton jumps known for bulk water, we observe that in contrast with what was reported for Ca-montmorillonite,[66] in a similar hydration state, these values are quite similar. This is in full agreement with the recent work of Petersen et al.[54] who showed that the interlayer water molecules are more liquid-like for lower net negative surface charge clay minerals.

(iv) Finally, the hypothesis that CO_2 may attach to the edge of some nickel hydroxide islands forming a strong bond can clarify the small decrease in the elastic signal and consequently slight increase in the quasi-elastic broadening after CO_2 exposure in dried Ni-Hec. Furthermore, by comparing the χ^2 obtained using the phenomenological method to that obtained using the minimal model approach,[54] Figure 8, we observe that these values are higher for hydrated Ni-Hec. This indicates that a more constrained water population, most likely belonging to the CO_2 attached to the hydroxide species, cannot be fully captured by the data, and further measurements using a higher-resolution spectrometer are needed.

Thus, we hypothesize that at the timescale probed using IRIS, the interstratified species contribute to a greater restriction of the water mobility, and a new confined water population in Ni-Hec develops upon CO_2 exposure.

https://doi.org/10.1021/acs.jpcc.2c03310
J. Phys. Chem. C 2022, 126, 17243−17254

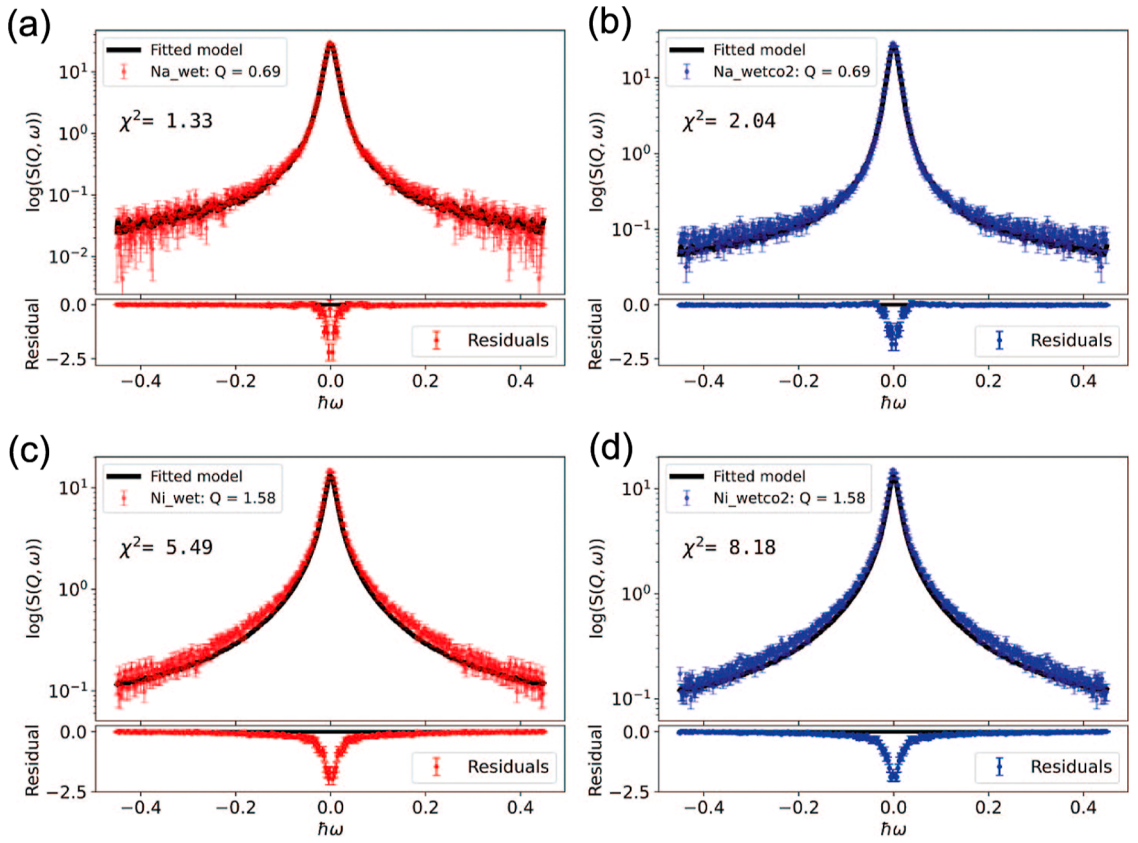

Figure 8. Experimental spectra of (a,b) Na-Hec and (c,d) Ni-Hec at different q-values fitted using the minimal model approach. A point to notice in (a,b) is that the fitted model follows the spectra very well. The reason for this behavior is that a single relaxation can describe the water dynamics in this sample. On the other hand, contributions originating from different water molecule populations that coexist in the interlayer contribute to the dynamics observed, which explains the deviation between the model and the experimental data in (c,d).

DFT Calculations. DFT calculations enabled the evaluation of the electrostatic environment involved in the adsorption of CO_2 in the interlayer region. From the simulations, we obtain an equilibrium d-spacing of 11.9 Å in which the CO_2 molecule remains linear and parallel to the clay surface (Figure 9), in line with NMR results[20] and simulations.[32,38,39] The equilibrium d-spacing value is close to the one observed experimentally for 1WL (12.2 Å), which reveals the important role of water in the clay swelling when exposed to CO_2. In agreement with previous[11,18,24,32,33] and current experimental results, compared to the dried state (d-spacing equal to 9.1 Å), the water layer decreases the cohesion energy for the layer expansion and creates the physical space for the CO_2 intercalation.

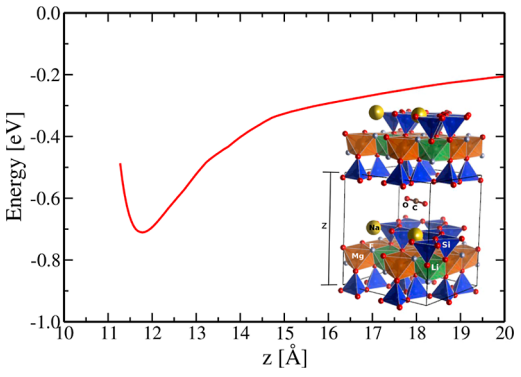

Figure 9. Energy curve as a function of the Hec layer separation, considering a single CO_2 molecule in the interlayer space. The well depth may be interpreted as the cohesion energy per unit cell, while the minimum energy point position is the equilibrium d-spacing for the molecular configuration depicted in the inset panel.

We also evaluated the hydration features in the confinement space. As a consequence of the water exposure, the Na interlayer atom leaves the cavity in the Hec structure to display an out-of-plane configuration (Figure 10a). Also, the water molecules may surround the Na atom, so they can form hydrogen bonds with the exposed clay's surface oxygen. To better understand the electrostatic environment of the interlayer space, we evaluated the charge rearrangements resulting from the substitutional atom considering eq 1. For this given atomic arrangement, the clay surface may display important electronic structure rearrangement. Indeed, the charge accumulation resulting from the substitutional atom (Li) mainly affects the nearest clay surface oxygens, favoring the electrostatic interaction with the water hydrogens (Figure 10b).

Due to the confined environment (Figure 11a), the Na hydration number is reduced compared to that in a bulk aqueous solution. The Na atom may interact with up to four water molecules instead of six, albeit a coordination number of 3 being the most common observed configuration. Additional water molecules attach to the hydrated compound through hydrogen bonds (see Figure 11b), in line with previous experimental results.[27,67]

https://doi.org/10.1021/acs.jpcc.2c03310
J. Phys. Chem. C 2022, 126, 17243−17254

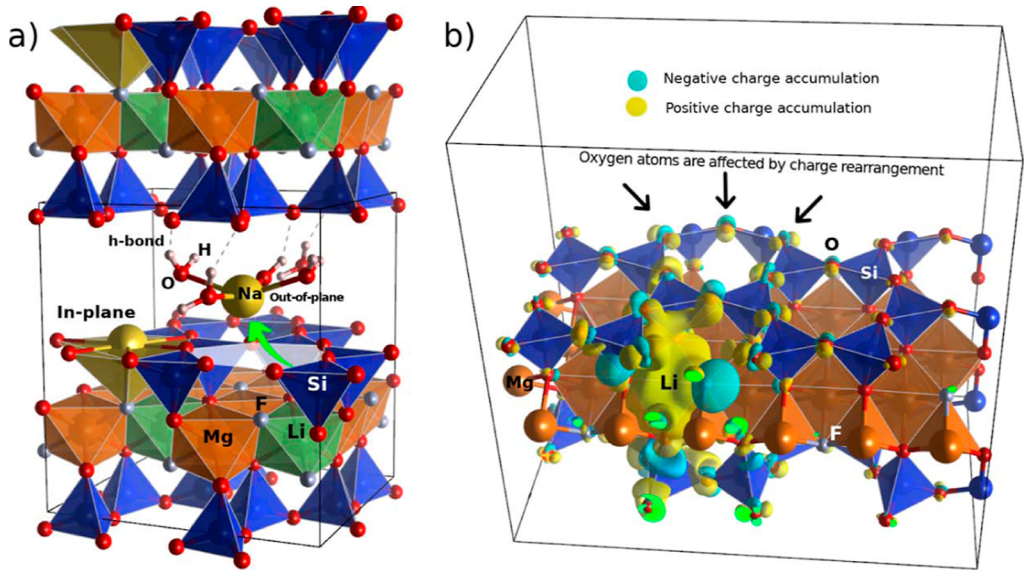

Figure 10. (a) Hydrated compound confined in Hec interlayer space. This figure highlights the out-of-plane configuration resulting from the Na hydration and the formation of hydrogen bonds between the water molecules and the clay's surface oxygen atoms. (b) Charge rearrangement as a consequence of substitutional atom (Li). The isosurfaces ($\pm$0.005 e/Å^3) were determined following eq 1. The oxygen atoms are the ones most affected, which may contribute to the polar character responsible for the H-bonds.

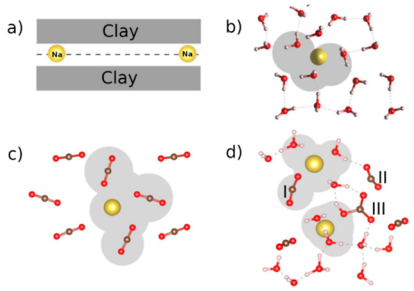

Figure 11. Snapshots are taken from the ab initio molecular dynamics simulations for confined fluids in the Na-Hec interlayer space (*d*-spacing 12.2 Å). (a) illustrates the side view, and (b–d) are top views of representative molecular conformations for H_2O, CO_2, and their mixture, respectively. Gray regions highlight the sodium first coordination shell. (d) signals three possible molecular conformations for CO_2: I-directly adsorbed on Na, II-interacting with water molecules, and III-interacting with a hydroxide.

Similarly, we also evaluated the adsorption of CO_2 molecules with the interlayer Na atom. In this case, Na may accept up to three CO_2 molecules (Figure 11c), with an adsorption energy of -0.58 ± 0.05 eV determined using eq 2. This is lower than that for the water adsorption case where it was determined to be -1.23 ± 0.3 eV.

Finally, we considered the scenario with both CO_2 and H_2O in the interlayer space to evaluate the adsorption features with this mixture (Figure 11d). The Na atom may accept CO_2 molecules if their hydration number is up to 3 (Figure 11d, I). Indeed, CO_2 attachment to the Na atom is possible if it is partially hydrated since the H_2O/CO_2 exchange is not energetically favorable. Also, the interaction between CO_2 and the hydrated compound occurs via the water hydrogens (Figure 11d, II). Interestingly, the dynamics of proton transfer through hydrogen bonds (previously observed by NMR[67]) may result in the formation of a hydroxide, and the CO_2 molecules may adsorb there (Figure 11d, III). The molecular bending features (deformation angle larger than 120) and the proximity to OH suggest that carbonate formation may occur.

CONCLUSIONS

Using X-ray powder diffraction, neutron spectroscopy, and DFT simulations, we have studied CO_2 exposure of a clay mineral from the perspective of the interlayer water. The investigations highlight the molecular interactions between CO_2 and water within the 2D interlayer of synthetic hectorite. Study of high-purity synthetic samples brings out important aspects that also apply to their natural counterparts without the interference of impurities and defects. As opposed to Ni-Hec where a swelling was observed for both the hydrated and dehydrated state exposed to CO_2, no swelling was observed for Na-Hec in the 0 WL and 1 WL state. This confirms previous observations that fully collapsed clay interlayers do not accept CO_2 in their interlayers. For Na-Hec hydrated at 1 WL, we observe damping of the librational modes associated with the intercalated water, suggesting that the interaction with CO_2 disrupts the H-bonding network of intercalated water. This, in turn, results in a modified confined water population, which is observed for both Ni-Hec and Na-Hec. For Ni-Hec, previous results demonstrating that CO_2 attaches to the edge of nickel hydroxide islands in the interlayer were confirmed by a small decrease in the elastic signal and consequently a slight increase in the quasi-elastic broadening after CO_2 exposure. Finally, the DFT calculations agree with previous and current experimental results in that intercalated water decreases the layer–layer cohesion energy and creates physical space for CO_2 intercalation. The DFT calculations further confirmed that interlayer confinement reduces the Na^+ hydration number compared to bulk aqueous water. This may allow for proton transfer and associated hydroxide formation that could adsorb CO_2 in the form of carbonates. The latter is corroborated by the present experimental results.

https://doi.org/10.1021/acs.jpcc.2c03310
J. Phys. Chem. C 2022, 126, 17243–17254

■ ASSOCIATED CONTENT

Supporting Information

The Supporting Information is available free of charge at https://pubs.acs.org/doi/10.1021/acs.jpcc.2c03310.

Supporting measurements by neutron powder diffraction and additional QENS data (PDF)

■ AUTHOR INFORMATION

Corresponding Authors

Kristoffer W. Bø Hunvik − *Department of Physics, Norwegian University of Science and Technology, Trondheim 7491, Norway;* orcid.org/0000-0002-2684-6464; Email: kristoffer.hunvik@ntnu.no

Jon Otto Fossum − *Department of Physics, Norwegian University of Science and Technology, Trondheim 7491, Norway;* orcid.org/0000-0002-8952-303X; Email: jon.fossum@ntnu.no

Heloisa N. Bordallo − *Niels Bohr Institute, University of Copenhagen, Copenhagen 1017, Denmark; European Spallation Source ESS ERIC, Lund 224 84, Sweden;* orcid.org/0000-0003-0750-0553; Email: bordallo@nbi.ku.dk

Authors

Rodrigo José da Silva Lima − *Academic Unit of Physics, Federal University of Campina Grande, Campina Grande 58429-900 Paraíba, Brazil;* orcid.org/0000-0003-1528-845X

Alexsandro Kirch − *Departamento de Física dos Materiais e Mecânica, Instituto de Física, Universidade de São Paulo, São Paulo 05508-090, São Paulo, Brasil*

Patrick Loch − *Bavarian Polymer Institute and Department of Chemistry, University of Bayreuth, Bayreuth 95447, Germany*

Paul Monceyron Røren − *Department of Physics, Norwegian University of Science and Technology, Trondheim 7491, Norway*

Martin Hoffmann Petersen − *Niels Bohr Institute, University of Copenhagen, Copenhagen 1017, Denmark*

Svemir Rudić − *ISIS Neutron and Muon Source, Rutherford Appleton Laboratory, STFC, Didcot OX11 0QX, U.K.;* orcid.org/0000-0003-3023-8565

Victoria García Sakai − *ISIS Neutron and Muon Source, Rutherford Appleton Laboratory, STFC, Didcot OX11 0QX, U.K.*

Kenneth Dahl Knudsen − *Institute for Energy Technology (IFE), Kjeller 2007, Norway; Department of Physics, Norwegian University of Science and Technology, Trondheim 7491, Norway*

Caetano Rodrigues Miranda − *Departamento de Física dos Materiais e Mecânica, Instituto de Física, Universidade de São Paulo, São Paulo 05508-090, São Paulo, Brasil*

Josef Breu − *Bavarian Polymer Institute and Department of Chemistry, University of Bayreuth, Bayreuth 95447, Germany;* orcid.org/0000-0002-2547-3950

Complete contact information is available at: https://pubs.acs.org/10.1021/acs.jpcc.2c03310

Notes

The authors declare no competing financial interest.

■ ACKNOWLEDGMENTS

This work was supported by the Research Council of Norway under the Frinatek Program, project number 250728. Experiments at the ISIS Pulsed Neutron and Muon Source were supported by a beamtime allocation from the Science and Technology Facilities Council.[68,69] This work was supported by the Deutsche Forschungsgemeinschaft (SFB 840). P.L. thanks Elite Network Bavaria in the framework of the Elite Study Program "Macromolecular Science" for support. A.K. and C.R.M. gratefully acknowledge the Research Centre for Gas Innovation (RCGI), support from the Brazilian agencies FAPESP (2017/02317-2) and CNPq, and the resources supplied by the Center for Scientific Computing (NCC/GridUNESP) of São Paulo State University (UNESP). M.H.P. and H.N.B.'s work was funded by the Danish Agency for Science, Technology and Innovation through DANSCATT.

■ REFERENCES

(1) Bergaya, F.; Lagaly, G. *Handbook of Clay Science*; Newnes, 2013.

(2) Laird, D.; Barak, P.; Nater, E.; Dowdy, R. Chemistry of smectitic and illitic phases in interstratified soil smectite. *Soil Sci. Soc. Am. J.* **1991**, *55*, 1499−1504.

(3) Velde, B. Uses of clays. *Introduction to Clay Minerals*; Springer, 1992; pp 164−176.

(4) Kausar, A.; Iqbal, M.; Javed, A.; Aftab, K.; Nazli, H. N.; Bhatti, S.; et al. Dyes adsorption using clay and modified clay: a review. *J. Mol. Liq.* **2018**, *256*, 395−407.

(5) dos Santos, E.; Rozynek, Z.; Hansen, E. L.; Hartmann-Petersen, R.; Klitgaard, R.; Løbner-Olesen, A.; Michels, L.; Mikkelsen, A.; Plivelic, T. S.; Bordallo, H.; et al. Ciprofloxacin intercalated in fluorohectorite clay: identical pure drug activity and toxicity with higher adsorption and controlled release rate. *RSC Adv.* **2017**, *7*, 26537−26545.

(6) Viseras, C.; Cerezo, P.; Sanchez, R.; Salcedo, I.; Aguzzi, C. Current challenges in clay minerals for drug delivery. *Appl. Clay Sci.* **2010**, *48*, 291−295.

(7) dos Santos, E.; Gates, W.; Michels, L.; Juranyi, F.; Mikkelsen, A.; da Silva, G.; Fossum, J.; Bordallo, H. The pH influence on the intercalation of the bioactive agent ciprofloxacin in fluorohectorite. *Appl. Clay Sci.* **2018**, *166*, 288−298.

(8) Joshi, G. V.; Kevadiya, B. D.; Bajaj, H. C. Design and evaluation of controlled drug delivery system of buspirone using inorganic layered clay mineral. *Microporous Mesoporous Mater.* **2010**, *132*, 526−530.

(9) Sellin, P.; Leupin, O. X. The Use of Clay as an Engineered Barrier in Radioactive-Waste Management - A Review. *Clays Clay Miner.* **2013**, *61*, 477−498.

(10) Altmann, S.; Tournassat, C.; Goutelard, F.; Parneix, J.-C.; Gimmi, T.; Maes, N. Diffusion-driven transport in clayrock formations. *Appl. Geochem.* **2012**, *27*, 463−478.

(11) Mendel, N.; Sîretanu, D.; Sîretanu, I.; Brilman, D. W.; Mugele, F. Interlayer Cation-Controlled Adsorption of Carbon Dioxide in Anhydrous Montmorillonite Clay. *J. Phys. Chem. C* **2021**, *125*, 27159−27169.

(12) Busch, A.; Bertier, P.; Gensterblum, Y.; Rother, G.; Spiers, C.; Zhang, M.; Wentinck, H. M. On sorption and swelling of CO2 in clays. *Geomechanics and Geophysics for Geo-energy and Geo-resources* **2016**, *2*, 111−130.

(13) Ferrage, E.; Lanson, B.; Michot, L. J.; Robert, J.-L. Hydration properties and interlayer organization of water and ions in synthetic Na-smectite with tetrahedral layer charge. Part 1. Results from X-ray diffraction profile modeling. *J. Phys. Chem. C* **2010**, *114*, 4515−4526.

(14) Dazas, B.; Lanson, B.; Breu, J.; Robert, J.-L.; Pelletier, M.; Ferrage, E. Smectite fluorination and its impact on interlayer water content and structure: A way to fine tune the hydrophilicity of clay surfaces? *Microporous Mesoporous Mater.* **2013**, *181*, 233−247.

(15) Tenório, R. P.; Engelsberg, M.; Fossum, J. O.; da Silva, G. J. Intercalated water in synthetic fluorhectorite clay. *Langmuir* **2010**, *26*, 9703−9709.
(16) Hemmen, H.; Rolseth, E. G.; Fonseca, D. M.; Hansen, E. L.; Fossum, J. O.; Plivelic, T. S. X-ray studies of carbon dioxide intercalation in Na-fluorohectorite clay at near-ambient conditions. *Langmuir* **2012**, *28*, 1678−1682.
(17) Michels, L.; Fossum, J. O.; Rozynek, Z.; Hemmen, H.; Rustenberg, K.; Sobas, P. A.; Kalantzopoulos, G. N.; Knudsen, K. D.; Janek, M.; Plivelic, T. S.; et al. Intercalation and retention of carbon dioxide in a smectite clay promoted by interlayer cations. *Sci. Rep.* **2015**, *5*, 8775.
(18) Hunvik, K. W. B.; Loch, P.; Cavalcanti, L. P.; Seljelid, K. K.; Røren, P. M.; Rudić, S.; Wallacher, D.; Kirch, A.; Knudsen, K. D.; Rodrigues Miranda, C.; et al. CO2 Capture by Nickel Hydroxide Interstratified in the Nanolayered Space of a Synthetic Clay Mineral. *J. Phys. Chem. C* **2020**, *124*, 26222−26231.
(19) Giesting, P.; Guggenheim, S.; Koster van Groos, A. F. K.; Busch, A. Interaction of carbon dioxide with Na-exchanged montmorillonite at pressures to 640bars: Implications for CO2 sequestration. *Int. J. Greenh. Gas Control* **2012**, *8*, 73−81.
(20) Bowers, G. M.; Schaef, H. T.; Loring, J. S.; Hoyt, D. W.; Burton, S. D.; Walter, E. D.; Kirkpatrick, R. J. Role of cations in CO2 adsorption, dynamics, and hydration in smectite clays under in situ supercritical CO2 conditions. *J. Phys. Chem. C* **2017**, *121*, 577−592.
(21) Hwang, J.; Joss, L.; Pini, R. Measuring and modelling supercritical adsorption of CO2 and CH4 on montmorillonite source clay. *Microporous Mesoporous Mater.* **2019**, *273*, 107−121.
(22) Grekov, D. I.; Suzuki-Muresan, T.; Kalinichev, A. G.; Pré, P.; Grambow, B. Thermodynamic data of adsorption reveal the entry of CH4 and CO2 in a smectite clay interlayer. *Phys. Chem. Chem. Phys.* **2020**, *22*, 16727−16733.
(23) Schaef, H. T.; Loring, J. S.; Glezakou, V.-A.; Miller, Q. R.; Chen, J.; Owen, A. T.; Lee, M.-S.; Ilton, E. S.; Felmy, A. R.; McGrail, B. P.; et al. Competitive sorption of CO2 and H2O in 2:1 layer phyllosilicates. *Geochim. Cosmochim. Acta* **2015**, *161*, 248−257.
(24) Schaef, H. T.; Loganathan, N.; Bowers, G. M.; Kirkpatrick, R. J.; Yazaydin, A. O.; Burton, S. D.; Hoyt, D. W.; Thanthiriwatte, K. S.; Dixon, D. A.; McGrail, B. P.; et al. Tipping point for expansion of layered aluminosilicates in weakly polar solvents: supercritical CO2. *ACS Appl. Mater. Interfaces* **2017**, *9*, 36783−36791.
(25) Hwang, J.; Pini, R. Enhanced sorption of supercritical CO2 and CH4 in the hydrated interlayer pores of smectite. *Langmuir* **2021**, *37*, 3778−3788.
(26) Stöter, M.; Kunz, D. A.; Schmidt, M.; Hirsemann, D.; Kalo, H.; Putz, B.; Senker, J.; Breu, J. Nanoplatelets of Sodium Hectorite Showing Aspect Ratios of ≈20 000 and Superior Purity. *Langmuir* **2013**, *29*, 1280−1285.
(27) Kalo, H.; Milius, W.; Breu, J. Single crystal structure refinement of one- and two-layer hydrates of sodium fluorohectorite. *RSC Adv.* **2012**, *2*, 8452−8459.
(28) Marry, V.; Dubois, E.; Malikova, N.; Breu, J.; Haussler, W. Anisotropy of water dynamics in clays: Insights from molecular simulations for experimental QENS analysis. *J. Phys. Chem. C* **2013**, *117*, 15106−15115.
(29) Marry, V.; Dubois, E.; Malikova, N.; Durand-Vidal, S.; Longeville, S.; Breu, J. Water dynamics in hectorite clays: Infuence of temperature studied by coupling neutron spin echo and molecular dynamics. *Environ. Sci. Technol.* **2011**, *45*, 2850−2855.
(30) Larsen, S. R.; Michels, L.; dos Santos, É. C.; Berg, M. C.; Gates, W. P.; Aldridge, L. P.; Seydel, T.; Ollivier, J.; Telling, M. T.; Fossum, J.-O.; et al. Physicochemical characterisation of fluorohectorite: Water dynamics and nanocarrier properties. *Microporous Mesoporous Mater.* **2020**, *306*, 110512.
(31) Cavalcanti, L. P.; Kalantzopoulos, G. N.; Eckert, J.; Knudsen, K. D.; Fossum, J. O. A nano-silicate material with exceptional capacity for CO2 capture and storage at room temperature. *Sci. Rep.* **2018**, *8*, 11827.
(32) Loganathan, N.; Yazaydin, A. O.; Kirkpatrick, R. J.; Bowers, G. M. Tuning the Hydrophobicity of Layer-Structure Silicates To Promote Adsorption of Nonaqueous Fluids: Effects of F- for OH-Substitution on CO2 Partitioning into Smectite Interlayers. *J. Phys. Chem. C* **2019**, *123*, 4848−4855.
(33) Loganathan, N.; Bowers, G. M.; Yazaydin, A. O.; Kalinichev, A. G.; Kirkpatrick, R. J. Competitive Adsorption of H2O and CO2 in 2-Dimensional Nanoconfinement: GCMD Simulations of Cs- and Ca-Hectorites. *J. Phys. Chem. C* **2018**, *122*, 23460−23469.
(34) Loganathan, N.; Bowers, G. M.; Yazaydin, A. O.; Schaef, H. T.; Loring, J. S.; Kalinichev, A. G.; Kirkpatrick, R. J. Clay swelling in dry supercritical carbon dioxide: effects of interlayer cations on the structure, dynamics, and energetics of CO2 intercalation probed by XRD, NMR, and GCMD simulations. *J. Phys. Chem. C* **2018**, *122*, 4391−4402.
(35) Makaremi, M.; Jordan, K. D.; Guthrie, G. D.; Myshakin, E. M. Multiphase Monte Carlo and molecular dynamics simulations of water and CO2 intercalation in montmorillonite and beidellite. *J. Phys. Chem. C* **2015**, *119*, 15112−15124.
(36) Loganathan, N.; Yazaydin, A. O.; Bowers, G. M.; Kalinichev, A. G.; Kirkpatrick, R. J. Molecular dynamics study of CO2 and H2O intercalation in smectite clays: effect of temperature and pressure on interlayer structure and dynamics in hectorite. *J. Phys. Chem. C* **2017**, *121*, 24527−24540.
(37) Bø Hunvik, K. W.; Loch, P.; Wallacher, D.; Kirch, A.; Cavalcanti, L. P.; Rieß, M.; Daab, M.; Josvanger, V.; Grätz, S.; Yokaichiya, F.; et al. CO2 Adsorption Enhanced by Tuning the Layer Charge in a Clay Mineral. *Langmuir* **2021**, *37*, 14491−14499.
(38) Botan, A.; Rotenberg, B.; Marry, V.; Turq, P.; Noetinger, B. Carbon dioxide in montmorillonite clay hydrates: thermodynamics, structure, and transport from molecular simulation. *J. Phys. Chem. C* **2010**, *114*, 14962−14969.
(39) Sena, M. M.; Morrow, C. P.; Kirkpatrick, R. J.; Krishnan, M. Supercritical Carbon Dioxide at Smectite Mineral-Water Interfaces: Molecular Dynamics and Adaptive Biasing Force Investigation of CO2/H2O Mixtures Nanoconfined in Na-Montmorillonite. *Chem. Mater.* **2015**, *27*, 6946−6959.
(40) Martins, M. L.; Gates, W. P.; Michot, L.; Ferrage, E.; Marry, V.; Bordallo, H. N. Neutron scattering, a powerful tool to study clay minerals. *Appl. Clay Sci.* **2014**, *96*, 22−35.
(41) Parker, S. F.; Lennon, D.; Albers, P. W. Vibrational spectroscopy with neutrons: A review of new directions. *Appl. Spectrosc.* **2011**, *65*, 1325−1341.
(42) Jiménez-Ruiz, M.; Ferrage, E.; Blanchard, M.; Fernandez-Castanon, J.; Delville, A.; Johnson, M.; Michot, L. Combination of inelastic neutron scattering experiments and ab Initio quantum calculations for the study of the hydration properties of oriented Saponites. *J. Phys. Chem. C* **2017**, *121*, 5029−5040.
(43) Cygan, R. T.; Daemen, L. L.; Ilgen, A. G.; Krumhansl, J. L.; Nenoff, T. M. Inelastic neutron scattering and molecular simulation of the dynamics of interlayer water in smectite clay minerals. *J. Phys. Chem. C* **2015**, *119*, 28005−28019.
(44) Lima, R. J. S.; Okhrimenko, D. V.; Rudić, S.; Telling, M. T.; Sakai, V. G.; Hwang, D.; Barin, G.; Eckert, J.; Lee, J.-W.; Bordallo, H. N. Ammonia Storage in Hydrogen Bond-Rich Microporous Polymers. *ACS Appl. Mater. Interfaces* **2020**, *12*, 58161.
(45) Daab, M.; Eichstaedt, N. J.; Habel, C.; Rosenfeldt, S.; Kalo, H.; Schießling, H.; Förster, S.; Breu, J. Onset of Osmotic Swelling in Highly Charged Clay Minerals. *Langmuir* **2018**, *34*, 8215−8222.
(46) Loch, P.; Hunvik, K. W. B.; Puchtler, F.; Weiß, S.; Seljelid, K. K.; Røren, P. M.; Rudic, S.; Raaen, S.; Knudsen, K. D.; Bordallo, H. N.; et al. Spontaneous formation of an ordered interstratification upon Ni-exchange of Na-fluorohectorite. *Appl. Clay Sci.* **2020**, *198*, 105831.
(47) Jensen, T. R.; Nielsen, T. K.; Filinchuk, Y.; Jørgensen, J.-E.; Cerenius, Y.; Gray, E. M.; Webb, C. J. Versatilein situpowder X-ray diffraction cells for solid-gas investigations. *J. Appl. Crystallogr.* **2010**, *43*, 1456−1463.
(48) Pinna, R. S.; Rudić, S.; Parker, S. F.; Armstrong, J.; Zanetti, M.; Škoro, G.; Waller, S. P.; Zacek, D.; Smith, C. A.; Capstick, M. J.; et al.

The neutron guide upgrade of the TOSCA spectrometer. *Nucl. Instrum. Methods Phys. Res., Sect. A* **2018**, *896*, 68−74.
(49) Parker, S. F.; Fernandez-Alonso, F.; Ramirez-Cuesta, A. J.; Tomkinson, J.; Rudic, S.; Pinna, R. S.; Gorini, G.; Fernández Castañon, J. F. Recent and future developments on TOSCA at ISIS. *J. Phys.: Conf. Ser.* **2014**, *554*, 012003.
(50) Mitchell, P. C. H. *Vibrational Spectroscopy with Neutrons: With Applications in Chemistry, Biology, Materials Science and Catalysis*; World Scientific, 2005; Vol. 3.
(51) Arnold, O.; Bilheux, J.-C.; Borreguero, J.; Buts, A.; Campbell, S. I.; Chapon, L.; Doucet, M.; Draper, N.; Ferraz Leal, R. F.; Gigg, M.; et al. Mantid-Data analysis and visualization package for neutron scattering and μ SR experiments. *Nucl. Instrum. Methods Phys. Res., Sect. A* **2014**, *764*, 156−166.
(52) Carlile, C.; Adams, M. A. The design of the IRIS inelastic neutron spectrometer and improvements to its analysers. *Phys. B* **1992**, *182*, 431−440.
(53) Azuah, R. T.; Kneller, L. R.; Qiu, Y.; Tregenna-Piggott, P. L.; Brown, C. M.; Copley, J. R.; Dimeo, R. M. DAVE: a comprehensive software suite for the reduction, visualization, and analysis of low energy neutron spectroscopic data. *J. Res. Natl. Inst. Stand. Technol.* **2009**, *114*, 341.
(54) Petersen, M. H.; Vernet, N.; Gates, W. P.; Villacorta, F. J.; Ohira-Kawamura, S.; Kawakita, Y.; Arai, M.; Kneller, G.; Bordallo, H. N. Assessing Diffusion Relaxation of Interlayer Water in Clay Minerals Using a Minimalist Three-Parameter Model. *J. Phys. Chem. C* **2021**, *125*, 15085.
(55) Berg, M. C.; Benetti, A. R.; Telling, M. T.; Seydel, T.; Yu, D.; Daemen, L. L.; Bordallo, H. N. Nanoscale mobility of aqueous polyacrylic acid in dental restorative cements. *ACS Appl. Mater. Interfaces* **2018**, *10*, 9904−9915.
(56) Soler, J. M.; Artacho, E.; Gale, J. D.; García, A.; Junquera, J.; Ordejón, P.; Sánchez-Portal, D. The SIESTA method forab initioorder-Nmaterials simulation. *J. Phys.: Condens. Matter* **2002**, *14*, 2745.
(57) Berland, K.; Hyldgaard, P. Exchange functional that tests the robustness of the plasmon description of the van der Waals density functional. *Phys. Rev. B* **2014**, *89*, 035412.
(58) Li, J. Inelastic neutron scattering studies of hydrogen bonding in ices. *J. Chem. Phys.* **1996**, *105*, 6733−6755.
(59) Line, C. M.; Kearley, G. The librational and vibrational spectra of water in natrolite, Na2Al2Si3O10·2H2O compared with ab-initio calculations. *Chem. Phys.* **1998**, *234*, 207−222.
(60) Sobolev, O.; Le Forestier, L.; González, M. A.; Russina, M.; Kemner, E.; Cuello, G. J.; Charlet, L. Hydration of Na+, Ni2+, and Sm3+ in the interlayer of hectorite: A quasielastic neutron scattering study. *J. Phys. Chem. C* **2009**, *113*, 13801−13812.
(61) Rosenfeldt, S.; Stöter, M.; Schlenk, M.; Martin, T.; Albuquerque, R. Q.; Förster, S.; Breu, J. In-depth insights into the key steps of delamination of charged 2D nanomaterials. *Langmuir* **2016**, *32*, 10582−10588.
(62) Bowers, G. M.; Loring, J. S.; Schaef, H. T.; Cunniff, S. S.; Walter, E. D.; Burton, S. D.; Larsen, R. K.; Miller, Q. R.; Bowden, M. E.; Ilton, E. S.; et al. Chemical Trapping of CO2 by Clay Minerals at Reservoir Conditions: Two Mechanisms Observed by in Situ High-Pressure and -Temperature Experiments. *ACS Earth Space Chem.* **2019**, *3*, 1034−1046.
(63) Miskowiec, A.; Niedziela, J. L.; Kirkegaard, M. C.; Shields, A. E. Analysis of Water Coupling in Inelastic Neutron Spectra of Uranyl Fluoride. *Sci. Rep.* **2019**, *9*, 10476.
(64) Lewis, J. Gas Separation Membranes: Polymeric and Inorganic by AF Ismail, KC Khulbe, and T. Matsuura. *Chem. Eng. Educ.* **2018**, *52*, 223.
(65) Singwi, K.; Sjölander, A. Diffusive motions in water and cold neutron scattering. *Phys. Rev.* **1960**, *119*, 863.
(66) Ignazzi, R.; Gates, W. P.; Diallo, S. O.; Yu, D.; Juranyi, F.; Natali, F.; Bordallo, H. N. Electric field induced polarization effects measured by in situ neutron spectroscopy. *J. Phys. Chem. C* **2017**, *121*, 23582−23591.
(67) Tenório, R. P.; Alme, L. R.; Engelsberg, M.; Fossum, J. O.; Hallwass, F. Geometry and dynamics of intercalated water in Na-fluorhectorite clay hydrates. *J. Phys. Chem. C* **2008**, *112*, 575−580.
(68) Fossum, J. O.; Knudsen, K. D.; Rudic, S.; Hunvik, K. W. B.; Bordallo, H. N.; Røren, P. M. *Determining the Interaction between Water and Carbon Dioxide in Smectite Clay (INS)*; STFC ISIS Neutron and Muon Source, 2019.
(69) Fossum, J. O.; Hunvik, K. W.; Sakai, V. G.; Bordallo, H. N.; Knudsen, K. D.; Røren, P.; Petersen, M. *Determining the Interaction between Water and Carbon Dioxide in Smectite Clay (QENS)*; STFC ISIS Neutron and Muon Source, 2019.

https://doi.org/10.1021/acs.jpcc.2c03310
J. Phys. Chem. C 2022, 126, 17243−17254